State-Feedback Control of the SpaceHawk Earth-Based Lunar Hopper

Anthony Dzaba, Evan Mucasey, Andrew Abraham, Eugenio Schuster, and Terry Hart

***Abstract*—In this paper we present a control strategy for the SpaceHawk, an Earth-based model spacecraft designed to navigate the surface of the moon in a series of "hops". By design, the nonholonomic dynamics of the SpaceHawk allow the use of full-state feedback linearization, which obviates the need for more involved control techniques such as backstepping. We design two controllers: an exact feedback-linearization controller for the position states, and an approximate linearization controller for the attitude states. The approximate-linearization simplifies the attitude control task by excluding the highly nonlinear attitude dynamics from the designed control laws. Simulation results show both controllers performing well in stability and tracking.**

I. Introduction

Traditional planetary exploration vehicles falls into two classes: landers and rovers. Landers, such as the NASA Viking and Phoenix, are robotic spacecraft that use variable throttle rockets to perform a controlled decent onto a planetary surface. Once on the surface, the lander is free to explore the immediate vicinity of its landing zone but can not explore any regions beyond since it remains stationary for the duration of its mission. In contrast, rovers, such as the NASA Spirit and Opportunity, are generally delivered to the planetary surface by an external propulsion mechanism which is jettisoned once the decent is complete. Once on the planet, rovers utilizes some form of propulsion (typically powered wheels) to move along the surface of the planet. The rover is capable of exploring the area near its immediate landing site as well as areas within a few kilometers of the site. Rovers usually travel at very slow driving speeds and may take years to reach a target that is less than a kilometer away. For these reasons, traditional landers and rovers are inherently limited by their planetary exploration range.

In contrast, a hopper spacecraft has the ability to perform a controlled descent, complete valuable mission operations while landed, and then translate to a different location in a very short period of time [1]. To change landing sites, a hopper reignites its main engine in order to follow either a ballistic trajectory or horizontal hovering trajectory to its intended destination. This functionality offers grater mission flexibility and represents an enabling technology for exploring perilous terrain that traditional rovers are unable to traverse. Obstacles such as bolder fields, steep crater walls, mountains, and loose sand can all be bypassed by hopping [2], [3]. Additionally, like rotary wing aircraft, hoppers possess the ability to hold a stationary hover, allowing them to observe land features that are inaccessible to traditional landers and rovers.

Hopping spacecrafts date back to the mid 1960's with the advent of NASA's Survey program which attempted to soft-land seven robotic spacecraft on the surface of the Moon [4]. After its initial landing, Surveyor 6 reignited its vernier thrusters for 2.5 seconds, attained an altitude of roughly twelve feet, and translated roughly eight feet to the west before landing again on the lunar surface. This was the first liftoff of any craft from the surface of the moon. Recent developments include spacecraft simulator designs powered by ducted fans and compressed cold gas [5]. In this paper, we design a set of control laws for stabilizing the attitude and position of an Earth-based model lunar hopper. The SpaceHawk prototype has a 75 centimeter wingspan, a mass of 15 kilograms, a maximum thrust of 180 Newtons, and a maximum power draw of 13 kilowatts. The SpaceHawk is propelled by ducted fans mounted on single-axis gimbals which provide vectored thrust. The geometry of the SpaceHawk is similar to that of a quadrotor, a nonholonomic vehicle whose position must be controlled by modulating its attitude. Importantly, the additional actuation provided by the gimbals makes the SpaceHawk a quad-tiltrotor: a holonomic vehicle whose attitude and position can be controlled independently, presenting a more flexible control design problem.

This paper is organized as follows. In Section II, we derive a first principles model for the hopper's rigid-body dynamics. In Section III we present a feedback linearization control strategy. In Section IV, we present simulation results. Finally, in Section V, we discuss conclusions and future work.

II. Equations of Motion

The equations of motion of the SpaceHawk are derived in the inertial frame using the approach found in [6]. An image of the SpaceHawk prototype is given in Fig. 1. The inertial axes are separated from the Earth-fixed axes by a 3D translation vector and a scalar yaw rotation denoted ψ. The vehicle position is given by the vector $\xi = [x, y, z]^T$. The attitude is given by the Tait-Bryan angles $\eta = [\psi, \theta, \phi]^T$. In order to avoid ambiguities, the ranges of these angles are limited as follows:

$$\begin{array}{rcccl} -\pi & \leq & \psi & < & \pi, \\ -\pi/2 & \leq & \theta & \leq & \pi/2, \\ -\pi & \leq & \phi & < & \pi. \end{array} \tag{1}$$

A. Dzaba (anthony@lehigh.edu), E. Mucasey, A. Abraham, E. Schuster, and Terry Hart are with the Department of Mechanical Engineering & Mechanics, Lehigh University, Bethlehem, PA 18015 USA.

We define the Lagrangian

$$L(q,\dot{q}) = T_{trans} + T_{rot} + U, \tag{2}$$

$$q = [\xi, \eta]^T, \tag{3}$$

$$T_{trans} = \frac{m}{2}\dot{\xi}^T\dot{\xi}, \tag{4}$$

$$T_{rot} = \frac{1}{2}\Omega^T \mathbf{I}_{\xi\xi}\Omega, \tag{5}$$

$$U = -mgz, \tag{6}$$

$$\Omega = W_\Omega \dot{\eta}, \tag{7}$$

$$W_\Omega(\psi,\theta) = \begin{bmatrix} -\sin\theta & 0 & 1 \\ \cos\theta\sin\psi & \cos\psi & 0 \\ \cos\theta\cos\psi & -\sin\psi & 0 \end{bmatrix}, \tag{8}$$

$$\mathbf{I}_{\xi\xi} = \begin{bmatrix} I_{xx} & & \\ & I_{yy} & \\ & & I_{zz} \end{bmatrix}, \tag{9}$$

where $\mathbf{I}_{\xi\xi}$ is the moment of inertia tensor (which is assumed to contain only the principle moments of inertia, I_{jj}), m is the vehicle mass, g is the acceleration due to gravity, and Ω is the 3D angular rotation vector resolved in the body-fixed frame, which is separated from the inertial frame by the pitch and roll rotations θ and ϕ.

In (6), note that negative values of z represent positive altitude (and therefore increasing potential energy) because the z-axis of the inertial frame points toward the ground, in the direction of the Moon's gravitational force. The external forces, as resolved in the vehicle-fixed frame, are

$$F = \begin{bmatrix} F_x \\ F_y \\ -F_z \end{bmatrix} \triangleq \begin{bmatrix} f_{3_x} + f_{1_x} \\ f_{2_y} + f_{4_y} \\ -(f_{3_z} + f_{1_z}) - (f_{2_z} + f_{4_z}) \end{bmatrix}, \tag{10}$$

$$\tau = \begin{bmatrix} \tau_\psi \\ \tau_\theta \\ \tau_\phi \end{bmatrix} \triangleq \begin{bmatrix} (f_{3_x} - f_{1_x})l + (f_{2_y} - f_{4_y})l \\ (f_{2_z} - f_{4_z})l \\ (f_{3_z} - f_{1_z})l \end{bmatrix}, \tag{11}$$

where f_{i_j} are the scalar components of the fan thrust vectors, and l is the moment arm between opposing fans. Note that the z-component of the external force is negative semi-definite because the positive semi-definite cumulative thrust, F_z, is opposite in direction to the vehicle-fixed z-axis (which points toward the ground when the attitude is equal to zero). The vehicle-fixed axes and the external force vectors are illustrated in Fig. 2. Note that the eight two-term sums and differences on the right-hand side of (10) and (11) are eight independent equations in the eight scalar control inputs which compose the vector $f = \begin{bmatrix} f_1 & f_2 & f_3 & f_4 \end{bmatrix}^T$, where

$$f_1 = \begin{bmatrix} f_{1_x} \\ f_{1_z} \end{bmatrix} = \begin{bmatrix} f_1\sin\alpha_1 \\ f_1\cos\alpha_1 \end{bmatrix}, \tag{12}$$

$$f_2 = \begin{bmatrix} f_{2_y} \\ f_{2_z} \end{bmatrix} = \begin{bmatrix} f_2\sin\alpha_2 \\ f_2\cos\alpha_2 \end{bmatrix}, \tag{13}$$

$$f_3 = \begin{bmatrix} f_{3_x} \\ f_{3_z} \end{bmatrix} = \begin{bmatrix} f_3\sin\alpha_3 \\ f_3\cos\alpha_3 \end{bmatrix}, \tag{14}$$

$$f_4 = \begin{bmatrix} f_{4_y} \\ f_{4_z} \end{bmatrix} = \begin{bmatrix} f_4\sin\alpha_4 \\ f_4\cos\alpha_4 \end{bmatrix}, \tag{15}$$

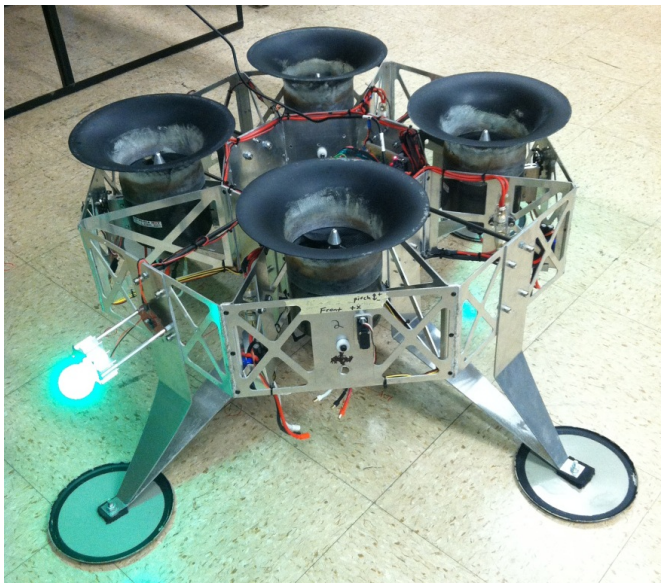

Figure 1. The SpaceHawk prototype features a heavy-duty aluminum frame and twenty-five centimeter fan cowlings.

and $-\frac{\pi}{2} < \alpha_i < \frac{\pi}{2}$ is the gimbal angle of the ith fan. These control inputs combine to exert a 3D force and a 3D moment on the vehicle. Realizing that this model has eight inputs for only six outputs, we can classify the SpaceHawk as an over-actuated system.

We map F from the vehicle-fixed frame to the inertial frame using the relation

$$F_\xi = R(\eta)F, \tag{16}$$

$$R(\eta) = \begin{bmatrix} c_\psi c_\theta & c_\theta s_\psi & -s_\theta \\ c_\psi s_\theta s_\phi - c_\phi s_\psi & c_\psi c_\phi + s_\psi s_\theta s_\phi & c_\theta s_\phi \\ s_\psi s_\phi + c_\psi c_\phi s_\theta & c_\phi s_\psi s_\theta - c_\psi s_\phi & c_\phi c_\theta \end{bmatrix}, \tag{17}$$

where $R(\eta)$ is the rotation matrix (intrinsic XYZ convention) from the body-fixed frame to the inertial frame. In (17), the trigonometric functions $\cos\alpha$ and $\sin\alpha$ have been abbreviated to c_α and s_α, respectively.

Evaluating the Lagrangian

$$\frac{d}{dt}\frac{\partial \mathcal{L}}{\partial \dot{q}} - \frac{\partial \mathcal{L}}{\partial q} = \begin{bmatrix} F_\xi \\ \tau \end{bmatrix}, \tag{18}$$

we obtain the equations of motion

$$m\ddot{\xi} + \begin{bmatrix} 0 \\ 0 \\ -mg \end{bmatrix} = R(\eta)F, \tag{19}$$

$$\mathbb{J}\ddot{\eta} + C(\eta,\dot{\eta})\dot{\eta} = \tau, \tag{20}$$

$$\mathbb{J}(\psi,\theta) = W_\Omega^T \mathbf{I}_{\xi\xi} W_\Omega, \tag{21}$$

$$C(\eta,\dot{\eta}) = \dot{\mathbb{J}} - \frac{1}{2}\frac{\partial}{\partial\eta}(\dot{\eta}^T\mathbb{J}), \tag{22}$$

where the six inputs are in $F \in R^3$ and $\tau \in R^3$.

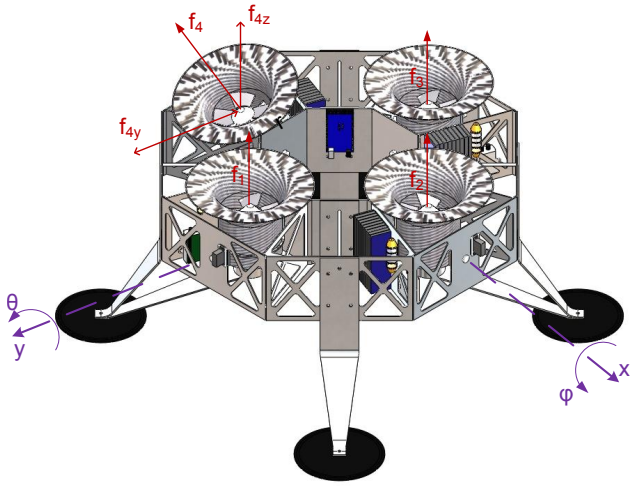

Figure 2. The free-body diagram of the SpaceHawk illustrates the individual thrust vectors (red) and the body fixed axes (purple).

III. Control Strategy

A. Feedback Linearization Analysis

In this section, the control objective is to track the twice differentiable reference functions $x_D(t)$, $y_D(t)$, $z_D(t)$, $\psi_D(t)$, $\theta_D(t)$, and $\phi_D(t)$, so that the errors defined by the outputs

$$\begin{bmatrix} x_e(t) \\ y_e(t) \\ z_e(t) \\ \psi_e(t) \\ \theta_e(t) \\ \phi_e(t) \end{bmatrix} \triangleq \begin{bmatrix} x(t) - x_D(t) \\ y(t) - y_D(t) \\ z(t) - z_D(t) \\ \psi(t) - \psi_D(t) \\ \theta(t) - \theta_D(t) \\ \phi(t) - \phi_D(t) \end{bmatrix}, \tag{23}$$

are stabilized at zero. Rearranging the equations of motion, (19) and (20), we have

$$\begin{bmatrix} \ddot{x} \\ \ddot{y} \\ \ddot{z} \end{bmatrix} = \frac{1}{m} R(\eta) \begin{bmatrix} F_x \\ F_y \\ -F_z \end{bmatrix} + \begin{bmatrix} 0 \\ 0 \\ g \end{bmatrix}, \tag{24}$$

$$\begin{bmatrix} \ddot{\psi} \\ \ddot{\theta} \\ \ddot{\phi} \end{bmatrix} = \mathbb{J}^{-1} \left(\begin{bmatrix} \tau_\psi \\ \tau_\theta \\ \tau_\phi \end{bmatrix} - C(\eta, \dot{\eta}) \begin{bmatrix} \dot{\psi} \\ \dot{\theta} \\ \dot{\phi} \end{bmatrix} \right). \tag{25}$$

We can use the state vector definitions

$$\beta = \begin{bmatrix} \beta_1 \\ \beta_2 \\ \beta_3 \\ \beta_4 \\ \beta_5 \\ \beta_6 \end{bmatrix} \triangleq \begin{bmatrix} x_e \\ y_e \\ z_e \\ \dot{x}_e \\ \dot{y}_e \\ \dot{z}_e \end{bmatrix}, \tag{26}$$

$$\delta = \begin{bmatrix} \delta_1 \\ \delta_2 \\ \delta_3 \\ \delta_4 \\ \delta_5 \\ \delta_6 \end{bmatrix} \triangleq \begin{bmatrix} \psi_e \\ \theta_e \\ \phi_e \\ \dot{\psi}_e \\ \dot{\theta}_e \\ \dot{\phi}_e \end{bmatrix}, \tag{27}$$

to convert the second-order subsystems, (24) and (25), into the first-order subsystems

$$\dot{\beta} = h_\beta(t, \beta, \delta, F), \tag{28}$$

$$\dot{\delta} = h_\delta(t, \delta, \tau), \tag{29}$$

$$h_\beta = \begin{bmatrix} \beta_4 \\ \beta_5 \\ \beta_6 \\ \frac{1}{m} R\left(\hat{\delta}\right) \begin{bmatrix} F_x \\ F_y \\ -F_z \end{bmatrix} - \begin{bmatrix} \ddot{x}_D(t) \\ \ddot{y}_D(t) \\ \ddot{z}_D(t) - g \end{bmatrix} \end{bmatrix}, \tag{30}$$

$$h_\delta = \begin{bmatrix} \delta_4 \\ \delta_5 \\ \delta_6 \\ \mathbb{J}^{-1} \left(\begin{bmatrix} \tau_\psi \\ \tau_\theta \\ \tau_\phi \end{bmatrix} - d \right) - \begin{bmatrix} \ddot{\psi}_D(t) \\ \ddot{\theta}_D(t) \\ \ddot{\phi}_D(t) \end{bmatrix} \end{bmatrix}, \tag{31}$$

$$\hat{\delta} = \begin{bmatrix} \delta_1 + \psi_D(t) \\ \delta_2 + \theta_D(t) \\ \delta_3 + \phi_D(t) \\ \delta_4 + \dot{\psi}_D(t) \\ \delta_5 + \dot{\theta}_D(t) \\ \delta_6 + \dot{\phi}_D(t) \end{bmatrix} = \begin{bmatrix} \psi \\ \theta \\ \phi \\ \dot{\psi} \\ \dot{\theta} \\ \dot{\phi} \end{bmatrix}, \tag{32}$$

$$d = C(\hat{\delta}) \begin{bmatrix} \hat{\delta}_4 \\ \hat{\delta}_5 \\ \hat{\delta}_6 \end{bmatrix}. \tag{33}$$

Subsystem (28), has three inputs in $\begin{bmatrix} F_x & F_y & F_z \end{bmatrix}^T$, and three outputs in $\begin{bmatrix} \beta_1 & \beta_2 & \beta_3 \end{bmatrix}^T$. Similarly, subsystem (29) has three inputs in $\begin{bmatrix} \tau_\psi & \tau_\theta & \tau_\phi \end{bmatrix}^T$, and three outputs in $\begin{bmatrix} \delta_1 & \delta_2 & \delta_3 \end{bmatrix}^T$. We note that (30) and (31) are both in the normal form with each subsystem having a relative degree of 2 in R^6. By observation, the zero dynamics for these subsystems show them to be minimum phase.

B. Control Design

We substitute the exact feedback linearization control law

$$\begin{bmatrix} F_x \\ F_y \\ F_z \end{bmatrix} \triangleq mR^{-1}(\hat{\delta}) \left(\begin{bmatrix} r_x \\ r_y \\ r_z \end{bmatrix} + \begin{bmatrix} \ddot{x}_D(t) \\ \ddot{y}_D(t) \\ \ddot{z}_D(t) - g \end{bmatrix} \right), \tag{34}$$

into (30) to obtain the decoupled, linearized position subsystem

$$\begin{bmatrix} \dot{\beta}_1 \\ \dot{\beta}_2 \\ \dot{\beta}_3 \\ \dot{\beta}_4 \\ \dot{\beta}_5 \\ \dot{\beta}_6 \end{bmatrix} = \begin{bmatrix} \beta_4 \\ \beta_5 \\ \beta_6 \\ r_x \\ r_y \\ r_z \end{bmatrix}, \tag{35}$$

where the control functions $\begin{bmatrix} r_x & r_y & r_z \end{bmatrix}^T$, have replaced $\begin{bmatrix} F_x & F_y & F_z \end{bmatrix}^T$ as the system inputs. We are now at liberty to apply linear control laws of our choosing to guarantee that the closed-loop position subsystem is globally exponentially stable.

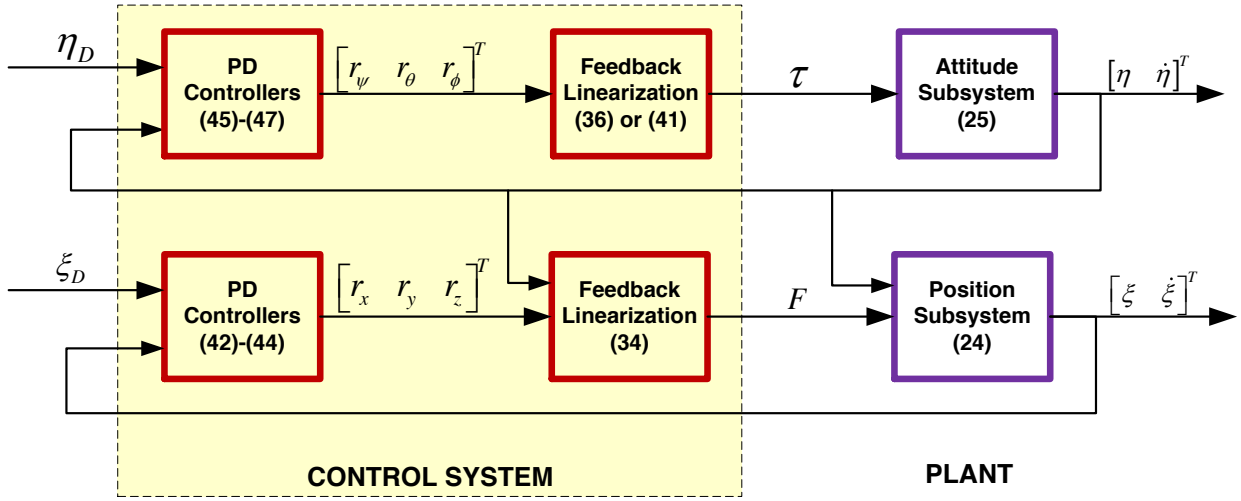

Figure 3. This input-output linearization block diagram shows how the cascade system (24)-(25) can be decoupled and stabilized using a combination of feedback linearization (or approximate linearization, see (41)) and proportional derivative (PD) control.

As with (34), we can substitute the exact feedback linearization control law

$$\begin{bmatrix} \tau_\psi \\ \tau_\theta \\ \tau_\phi \end{bmatrix} \triangleq C(\delta) \begin{bmatrix} \delta_4 \\ \delta_5 \\ \delta_6 \end{bmatrix} + \mathbb{J} \left(\begin{bmatrix} r_\psi \\ r_\theta \\ r_\phi \end{bmatrix} + \begin{bmatrix} \ddot{\psi}_D(t) \\ \ddot{\theta}_D(t) \\ \ddot{\phi}_D(t) \end{bmatrix} \right), \quad (36)$$

into (31) to obtain the linearized attitude subsystem

$$\begin{bmatrix} \dot{\delta}_1 \\ \dot{\delta}_2 \\ \dot{\delta}_3 \\ \dot{\delta}_4 \\ \dot{\delta}_5 \\ \dot{\delta}_6 \end{bmatrix} = \begin{bmatrix} \delta_4 \\ \delta_5 \\ \delta_6 \\ r_\psi \\ r_\theta \\ r_\phi \end{bmatrix}. \quad (37)$$

We note, however, that the computational expense of implementing the highly nonlinear (36) on an onboard microcontroller may be unjustified in light of the following. Since

$$\lim_{\delta \to 0} \mathbb{J} = \begin{bmatrix} I_{zz} & & \\ & I_{yy} & \\ & & I_{xx} \end{bmatrix}, \quad (38)$$

$$\lim_{\delta \to 0} \left(C(\delta) \begin{bmatrix} \delta_4 \\ \delta_5 \\ \delta_6 \end{bmatrix} \right) = 0, \quad (39)$$

near the origin, (31) becomes

$$\begin{bmatrix} \dot{\delta}_1 \\ \dot{\delta}_2 \\ \dot{\delta}_3 \\ \dot{\delta}_4 \\ \dot{\delta}_5 \\ \dot{\delta}_6 \end{bmatrix} = \begin{bmatrix} \delta_4 \\ \delta_5 \\ \delta_6 \\ \begin{bmatrix} I_{zz}^{-1} & & \\ & I_{yy}^{-1} & \\ & & I_{xx}^{-1} \end{bmatrix} \begin{bmatrix} \tau_\psi \\ \tau_\theta \\ \tau_\phi \end{bmatrix} - \begin{bmatrix} \ddot{\psi}_D(t) \\ \ddot{\theta}_D(t) \\ \ddot{\phi}_D(t) \end{bmatrix} \end{bmatrix}. \quad (40)$$

We can therefore drive δ_1, δ_2, and δ_3 to zero by applying the simpler approximate linearization control law

$$\begin{bmatrix} \tau_\psi \\ \tau_\theta \\ \tau_\phi \end{bmatrix} \triangleq \begin{bmatrix} I_{zz} & & \\ & I_{yy} & \\ & & I_{xx} \end{bmatrix} \left(\begin{bmatrix} r_\psi \\ r_\theta \\ r_\phi \end{bmatrix} + \begin{bmatrix} \ddot{\psi}_D(t) \\ \ddot{\theta}_D(t) \\ \ddot{\phi}_D(t) \end{bmatrix} \right). \quad (41)$$

We proceed by selecting a class of critically-damped PD controllers in

$$r_x \triangleq -2k_x\beta_4 - k_x^2\beta_1, \quad (42)$$
$$r_y \triangleq -2k_y\beta_5 - k_y^2\beta_2, \quad (43)$$
$$r_z \triangleq -2k_z\beta_6 - k_z^2\beta_3, \quad (44)$$
$$r_\psi \triangleq -2k_\psi\delta_4 - k_\psi^2\delta_1, \quad (45)$$
$$r_\theta \triangleq -2k_\theta\delta_5 - k_\theta^2\delta_2, \quad (46)$$
$$r_\phi \triangleq -2k_\phi\delta_6 - k_\phi^2\delta_3, \quad (47)$$

where k_x, k_y, k_z, k_ψ, k_θ, and k_ϕ are positive definite control gains. Substituting (45)-(47) into (37), we have

$$\dot{\delta} = A\delta, \quad (48)$$

$$A = \begin{bmatrix} 0 & 0 & 0 & 1 & 0 & 0 \\ 0 & 0 & 0 & 0 & 1 & 0 \\ 0 & 0 & 0 & 0 & 0 & 1 \\ -k_\psi^2 & 0 & 0 & -2k_\psi & 0 & 0 \\ 0 & -k_\theta^2 & 0 & 0 & -2k_\theta & 0 \\ 0 & 0 & -k_\phi^2 & 0 & 0 & -2k_\phi \end{bmatrix}, \quad (49)$$

for which the eigenvalues are $\lambda = -\begin{bmatrix} k_\psi & k_\psi & k_\theta & k_\theta & k_\phi & k_\phi \end{bmatrix}$. By virtue of Lyapunov's indirect method, we assert that the closed-loop attitude subsystem is therefore asymptotically stable in a neighborhood D, surrounding the origin [7].

Sampling Time	T	$0.01\,\mathrm{s}$
Fan Separation Distance	l	$0.75\,\mathrm{m}$
Vehicle Mass	m	$15\,\mathrm{Kg}$
Acceleration Due to Gravity on the Moon	g	$1.62\,\mathrm{m/s^2}$
Principle Moments of Inertia	I_{xx}	$0.541\,\mathrm{Kgm^2}$
	I_{yy}	$0.538\,\mathrm{Kgm^2}$
	I_{zz}	$0.872\,\mathrm{Kgm^2}$
Control Gains	k_x	1
	k_y	10
	k_z	2.25
	k_ψ	10
	k_θ	10
	k_ϕ	10

Table I
SIMULATION PARAMETERS

C. Control Implementation

During the control analysis, we selected $F \in R^3$ and $\tau \in R_3$ as our virtual inputs. These are functions of the eight scalar fan forces $\left[\begin{array}{cccccccc} f_{1_x} & f_{1_z} & f_{2_y} & f_{2_z} & f_{3_x} & f_{3_z} & f_{4_y} & f_{4_z} \end{array}\right]^T$. If we use (10) and (11) to express F and τ in matrix form, we can invert the matrix to solve for the scalar fan forces in terms of the control laws designed for F and τ. Noting that there are eight fan force inputs for only six inputs in F and τ, we avoid encountering a non-square matrix by defining two additional constraints. We choose to equally distribute both the cumulative thrust and the cumulative yawing moment between one pair of opposing fans and the other. These constraints, expressed mathematically as

$$(f_{3_z} + f_{1_z}) \triangleq (f_{2_z} + f_{4_z}), \quad (50)$$
$$(f_{3_x} - f_{1_x}) \triangleq (f_{2_y} - f_{4_y}), \quad (51)$$

allow us to rewrite (10) and (11) as

$$P = MU, \quad (52)$$
$$P = \left[\begin{array}{cccccccc} F_x & F_y & F_z & \tau_\psi & \tau_\theta & \tau_\phi & 0 & 0 \end{array}\right]^T, \quad (53)$$
$$U = \left[\begin{array}{cccccc} f_{1_x} & f_{1_z} & f_{2_y} & f_{2_z} & f_{3_x} & f_{3_z} \\ f_{4_y} & f_{4_z} \end{array}\right]^T, \quad (54)$$

$$M = \left[\begin{array}{cccccccc} 1 & 0 & 0 & 0 & 1 & 0 & 0 & 0 \\ 0 & 0 & 1 & 0 & 0 & 0 & 1 & 0 \\ 0 & 1 & 0 & 1 & 0 & 1 & 0 & 1 \\ -l & 0 & l & 0 & l & 0 & -l & 0 \\ 0 & 0 & 0 & l & 0 & 0 & 0 & -l \\ 0 & -l & 0 & 0 & 0 & l & 0 & 0 \\ 0 & 1 & 0 & -1 & 1 & 0 & 0 & -1 \\ -1 & 0 & -1 & 0 & 1 & 0 & 1 & 0 \end{array}\right], \quad (55)$$

where M is a 8x8 square matrix. Solving for the fan forces, we find

$$U = M^{-1}P, \quad (56)$$

$$\left[\begin{array}{c} f_{1_x} \\ f_{1_z} \\ f_{2_y} \\ f_{2_z} \\ f_{3_x} \\ f_{3_z} \\ f_{4_y} \\ f_{4_z} \end{array}\right] = \left[\begin{array}{c} \frac{1}{2}F_x - \frac{1}{4l}\tau_\psi \\ \frac{1}{4}F_z - \frac{1}{2l}\tau_\phi \\ \frac{1}{2}F_y + \frac{1}{4l}\tau_\psi \\ \frac{1}{4}F_z + \frac{1}{2l}\tau_\theta \\ \frac{1}{2}F_x + \frac{1}{4l}\tau_\psi \\ \frac{1}{4}F_z + \frac{1}{2l}\tau_\phi \\ \frac{1}{2}F_y - \frac{1}{4l}\tau_\psi \\ \frac{1}{4}F_z - \frac{1}{2l}\tau_\theta \end{array}\right]. \quad (57)$$

Next, we convert the eight scalar fan forces into four 2D fan thrusts where each thrust vector is composed of a scalar fan thrust magnitude and a scalar gimbal angle. For the ith fan these are

$$|f_i| = || \left[\begin{array}{c} f_{i_x} \\ f_{i_z} \end{array}\right] ||_2, \forall i = \{1,3\}, \quad (58)$$
$$|f_i| = || \left[\begin{array}{c} f_{i_y} \\ f_{i_z} \end{array}\right] ||_2, \forall i = \{2,4\}, \quad (59)$$
$$\alpha_i = \arctan \frac{f_{i_x}}{f_{i_z}}, \forall i = \{1,3\}, \quad (60)$$
$$\alpha_i = \arctan \frac{f_{i_y}}{f_{i_z}}, \forall i = \{2,4\}. \quad (61)$$

Lastly, we convert the thrust magnitudes, $|f_i|$, into the real inputs of the physical plant, which are the motor throttle values. To do this, each ducted fan is rigidly mounted on a custom force gauge (so that the gimbal angle does not come into play). Open-loop throttle commands are sent to the fan's electronic speed controller (ESC) while the corresponding thrust measurements are logged for offline identification. This process allows us to empirically estimate the motor velocity constant, K_V, which relates motor voltage to motor speed, and therefore to motor thrust.

IV. SIMULATION

Simulations of the dynamics model given in Section II, are carried out in Simulink. Fig. (4) shows the closed-loop system executing a short distance hopping maneuver. In the position response, the absences of overshoot and steady-state error demonstrate the efficacy of the feedback linearization control strategy. The attitude response is also quite good despite the initial conditions starting far from the origin. Here we find justification for choosing the simpler approximate feedback linearization controller, (41), over the more complex exact feedback linearization controller, (36). The critically damped PD controllers allow us to control the rise-time for each state through the control gains $k_{(\cdot)}$. For a given state, increasing the control gain will have the effect of increasing the expended control energy.

V. CONCLUSIONS

The feedback linearization control strategy showed good stability performance in simulation. We were able to demonstrate that in certain portions of the state space (near hover), we can set aside more complex nonlinear control laws in favor of simpler control laws which make the state equations pseudo-linear. The results show that appropriate choosing of which nonlinearities to cancel and which to allow, can create simple, efficient controllers with good stability and tracking performance. These controllers are high yield in terms of their performance payoff versus design time and implementation effort. Future work will include experiments designed to test the control performance in six degree of freedom (DOF) flight. Once we can demonstrate stability in the complete 6DOF pose, we will pursue advanced motion control objectives for optimizing the hopping process.

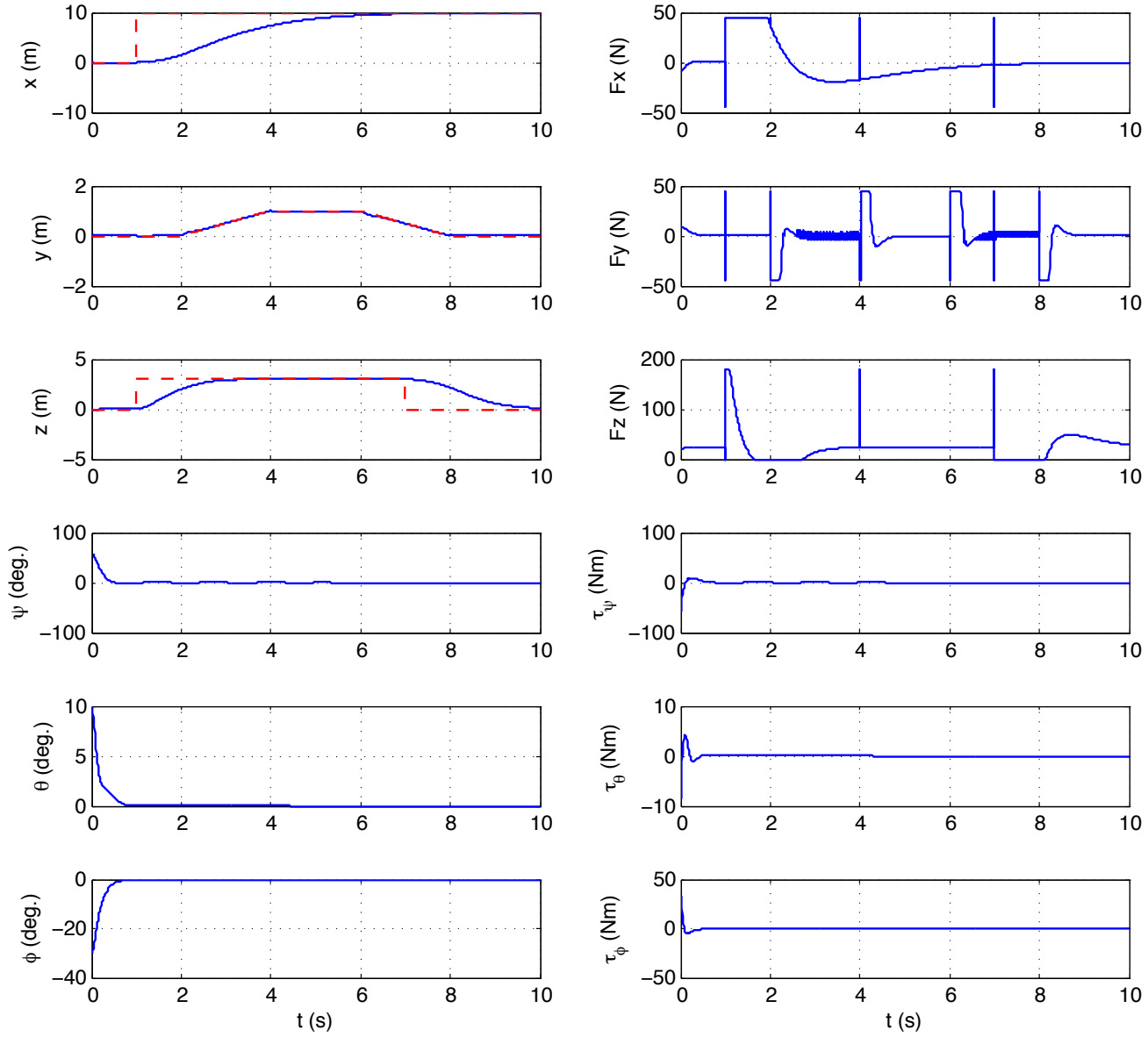

Figure 4. The plots on the left show the closed-loop response of the system (35), (37). In the position plots, the outputs (blue traces) track the the reference signals $\begin{bmatrix} x_D(t) & y_D(t) & z_D(t) \end{bmatrix}^T$ (red dashed traces). In the attitude plots, the outputs are stabilized at the origin arbitrarily fast with minimal overshoot and minimal steady-state error. The plots on the right show the corresponding trajectories of the control inputs.

REFERENCES

[1] E. R. Lanford, "Unique abilities of hopper spacecraft to enable national objectives for solar system exploration," Master's thesis, Massachusetts Institute of Technology, January 2006.

[2] A. J. Middleton, "Modeling and vehicle performance analysis of earth and lunar hoppers," Master's thesis, Massachusetts Institute of Technology, October 2010.

[3] P. M. Cunino, F. Alibay, P. Meira, T. Sheerin, E. Lanford, E. Krupczak, and J. A. Hoffman, "Options in the solar system for planetary surface exploration via hopping," in *Aerospace Conference, 2011 IEEE*, Massachusetts Institute of Technology 77 Massachusetts Ave Cambridge, MA 02139, 2011.

[4] R. Godwin, Ed., *Surveyor: Lunar Exploration Program, The NASA Mission Reports*. Apogee Books Box 62034 Burlington, Ontario, Canada: Apogee Books, 2006.

[5] S. L. Nothnagel, "Development of a cold gas propulsion system for the talaris hopper," Master's thesis, Massachusetts Institute of Technology, June 2011.

[6] P. Castillo, R. Lozano, and A. Dzul, "Stabilization of a mini rotorcraft with four rotors," *Control Systems, IEEE*, vol. 25, no. 6, pp. 45 – 55, dec 2005.

[7] H. Khalil, *Nonlinear Systems*. Prentice Hall, Jan. 2002. [Online]. Available: http://www.worldcat.org/isbn/0131227408

[8] P. Castillo, *Modelling and control of mini flying machines*. Springer-Verlag, 2005.

[9] P. M. Cunio, A. Babuscia, Z. J. Bailey, H. Chaurasia, R. Goel, A. A. Golkar, D. Selva, E. Timmons, B. E. Cohanim, J. A. Hoffman, and D. W. Miller, "Initial development of an earth-based prototype for a lunar hopper autonomous exploration system," in *AIAA Space 2009 Conference and Exposition*, Pasadena, CA, United states, 2009.

[10] A. Middleton and S. Paschall, "Development and deployment of a performance model for the prototype planetary exploration hopper," in *Aerospace Conference, 2011 IEEE*, march 2011, pp. 1 –6.

[11] A. Middleton, S. Paschall, and B. Cohanim, "Small lunar lander/hopper performance analysis," in *Aerospace Conference, 2010 IEEE*, march 2010, pp. 1 –7.

[12] M. X. Wendelin, "Use and sizeing of rocket hoppers for planetary surface exploration," Master's thesis, Massachusetts Institute of Technology, June 2010.